IEEE Access
Multidisciplinary | Rapid Review | Open Access Journal

Received November 25, 2019, accepted December 9, 2019, date of publication December 13, 2019,
date of current version December 26, 2019.

Digital Object Identifier 10.1109/ACCESS.2019.2959603

Sub-6GHz 4G/5G Conformal Glasses Antennas

YAN-YAN WANG[1], YONG-LING BAN[1], AND YANHUI LIU[2], (Senior Member, IEEE)
[1]School of Electronic Science and Engineering, University of Electronic Science and Technology of China, Chengdu 611731, China
[2]Global Big Data Technologies Centre, University of Technology Sydney, Ultimo, NSW 2007, Australia

Corresponding author: Yong-Ling Ban (byl@uestc.edu.cn)

This work was supported in part by the National Natural Science Foundation of China under Grant 61971098, and in part by the Fundamental Research Funds for the Central Universities under Grant ZYGX2018J037.

ABSTRACT The difficulty of antenna design applied to glasses is that the structure of glasses is too single, and the space available for antenna design is greatly limited. In this background, the integrated design of 4G antennas and 5G antennas applied to glasses is proposed in this paper. The most important highlight of this design is that it makes full use of the limited three-dimensional space structure provided by glasses and achieves the perfect combination of the antenna and glasses in the physical structure. Specifically, two antennas for 4G communication are arranged on two glasses frames, and four antennas for 5G communication are arranged on two glasses legs. In this way, we can make full use of the space provided by the glasses to design antennas and ensure that there is a certain distance between the 4G antennas and 5G antennas so that the performance of both 4G antennas and 5G antennas can be guaranteed. The 4G antenna consists of a loop structure printed on the frame and leg of the glasses and a parasitic branch strip printed on the front of the leg of the glasses. The resonance modes of the 4G antenna are mainly loop, monopole, and dipole modes, which can cover two 4G bands of 0.824-0.96 GHz and 1.71-2.69 GHz. Each 5G antenna mainly comes from the open slot mode etched on the metal ground surface of an FR4 substrate of the glasses leg. In addition, the slot antennas operate in two 5G bands of 3.3-3.6 GHz and 4.8-5.0 GHz. Finally, the glasses and the antennas are fabricated based on FR4 substrates and measured. The measured results show that the proposed antennas perform well and have the potential to be used in 4G/5G communications through glasses.

INDEX TERMS Smart glasses, wearable multiple-mode antenna, loop antenna, 4G, 5G.

I. INTRODUCTION

In recent years, wearable smart devices with wireless communication capabilities have received widespread attention, such as Google's smart glasses in 2012, Apple's smart watch in 2014, and LG's smart watch in 2015. Unfortunately, these early wearable smart devices only configure Bluetooth or WIFI antennas and can only indirectly connect to 3G/4G mobile networks carried on mobile phones through Bluetooth or WIFI. Early research on antennas in wearable smart devices also focused on Bluetooth or WIFI antennas [1]–[5], such as dual WIFI antennas on smart glasses [1] and multi Bluetooth antennas made of transparent materials [5].

Research on a wearable smart device 4G/LTE antenna directly connected to a mobile network has also been recently reported, and 4G/LTE antennas on wearable devices from some mainstream com-panies, including Apple, have also been developed. In [6], a three-port multi-band 4G antenna for smart watches is reported. The antenna is located in the watchband and metallic glass coating. 4G antennas used in smart eyewear have also appeared in five papers [7]–[11]. In [7], a simple eyewear 4G antenna is proposed for the first time. The antenna structure is printed on the leg of the eyewear. The optimal radiation efficiency of the antenna is approximately 14% in the low frequency band of 700-960 MHz and 36% in the high frequency band of 1.7 GHz-2.7 GHz. In [8], the working principle of this eyewear antenna is further analyzed by means of the characteristic mode theory. In [9], the influence of a metal frame loaded around a head on the performance of the eyewear antenna is studied. In [11], an eyewear frame composed of an ABS (acrylonitrile-butadiene-styrene) plastic medium was fabricated by three-dimensional printing technology, and a 4G eyewear antenna was then designed and measured.

These 4G antennas, which can be used in wearable smart devices, can cover the common band of 4G, but only a single antenna is designed, which obviously does not meet the requirements of a multi-antenna configuration for

The associate editor coordinating the review of this manuscript and approving it for publication was Hassan Tariq Chattha.

4G MIMO communication. In addition, with the landing of 5G communication standards and the promotion of 5G industrialization, it is necessary to carry out research work that is applicable deploying 5G antennas simultaneously on wearable smart devices.

The difficulty of antenna design applied to glasses is that the structure of glasses is too single and the space available for antenna design is greatly limited. The antennas [7]–[11] used in glasses are mostly placed on the glasses legs. If we consider the design of 4G MIMO dual antennas and 5G MIMO antennas at the same time, it is obvious that the space for antenna on the glasses is not large enough. Therefore, the integrated design of 4G antennas and 5G antennas in glasses will be full of challenges.

5G communication technology with higher transmission rate and larger capacity has become the technology that mobile terminal equipment (including wearable smart glasses, etc.) must study in the future. The antenna design of 5G mobile terminal will become a great demand. Considering the compatibility of communication system, 4G communication technology will coexist with 5G communication technology for a long time. In this paper, 4G antennas and 5G antennas are designed on smart glasses. It can not only meet the current 4G communication requirements, but also play an important role in the 5G era in the future. In this background, the integrated design of 4G antennas and 5G antennas for glasses is proposed in this paper. The most important highlight of this design is that it makes full use of the limited three-dimensional space structure provided by glasses and achieves the perfect combination of antenna and glasses in the physical structure. Two antennas for 4G communication are arranged on two glasses frames, and four antennas for 5G communication are arranged on two glasses legs. In this way, we can make full use of the space provided by the glasses to design antennas and try to ensure that there is a certain distance between the 4G and 5G antennas so that the performance of both 4G and 5G antennas can be guaranteed. The structure of this paper is as follows. First, the design of the 4G antennas is discussed. Then, the design of the 5G antennas is discussed. A section concerning the influence of the human head on antenna performance follows. Finally, manufacturing and testing are discussed.

II. 4G/5G GLASSES ANTENNAS

Fig. 1 shows the overall structure of the 4G/5G antennas applied to the glasses and the detailed structure of the 4G antennas. All the antenna structures are printed on FR4 substrates of 1-mm thickness. The relative dielectric constant of FR4 substrate is 4.4, and the tangent of loss angle is 0.02. The size of the three-dimensional structure of the whole glasses is 166 mm × 100.5 mm × 44 mm. The glasses are in line with the current fashion. Each glasses frame is 62 mm × 44 mm in size, and there is an FR4 substrate with a size of 20 mm × 5 mm between the two glasses frames. The left and right glasses frames are connected together to form a symmetrical structure. The glasses legs are modeled as an

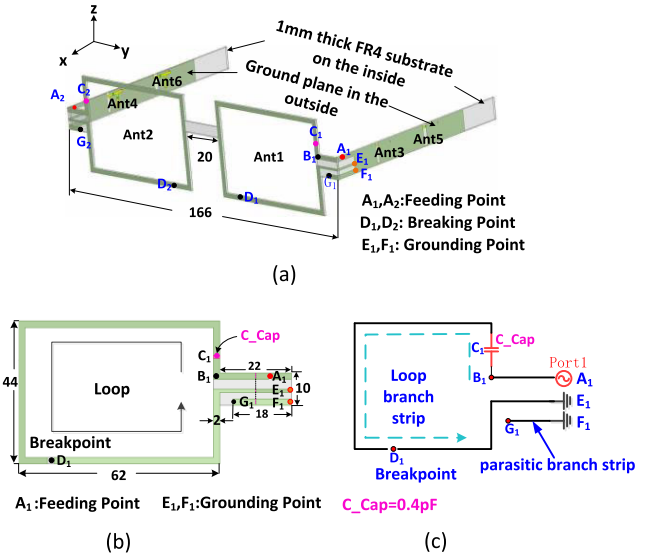

FIGURE 1. (a) Geometry of the proposed 4G/5G glasses antennas. (b) Detailed dimensions of the 4G antennas. (c) Equivalent structure of the proposed 4G antenna.

FR4 substrate with a size of 100.5 mm × 10 mm. The surface of the FR4 substrate is printed with a ground plane with a size of 69.5 mm × 10 mm. The size of the connecting part between the glasses frame and the glasses leg is 11 mm × 10 mm, which is convenient for the wearing of the glasses on the user's head. Two 4G antennas (Ant1 and Ant2) are printed on the glasses frame, and four 5G slot antennas (Ant3, Ant4, Ant5, and Ant6) are etched on the glasses legs.

A. 4G GLASSES ANTENNAS

The overall structure and specific size of the 4G glasses antenna are shown in Fig. 1 (b). Because of the symmetrical structure of antennas Ant1 and Ant2, only antenna Ant1 is shown here. The antenna Ant1 consists of two parts, one of which is a loop structure ($A_1 \rightarrow B_1 \rightarrow C_1 \rightarrow D_1 \rightarrow E_1 \rightarrow A_1$) printed on the frame and leg of the glasses, and the other is a parasitic branch strip F_1 G_1 printed on the front of the leg of the glasses, where A_1 is the feeding point, and E_1 and F_1 are the grounding points. There is a breakpoint of 2-mm width at the D_1 point of the loop structure. In addition, to tune the resonant frequencies of the antenna and improve the matching characteristics of the proposed antenna, a lumped capacitance C_cap is loaded at the C_1 point of the loop structure with a capacitance value of 0.4 pF [12], [13].

Next, HFSS V15 [14] is used to analyze the resonant modes of the proposed 4G glasses antennas. To clearly see the resonant structure of each resonant mode of the proposed antenna, the reference antennas Ref1 and Ref2 are introduced. The structure of the reference antenna Ref1 is not loaded with lumped capacitance C_cap relative to antenna Ant1, and the structure of reference antenna Ref2 has no parasitic branch strip F_1 G_1 relative to antenna Ant1. Fig. 2 shows the simulation results of S-parameters of Ant1, Ref1 and

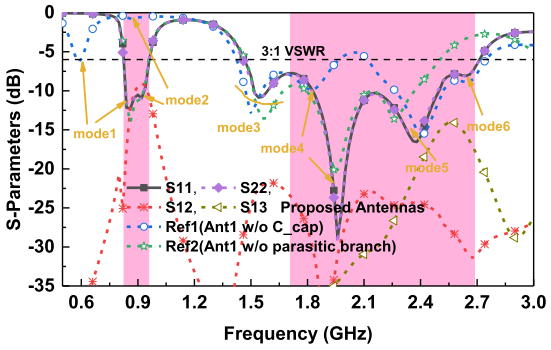

FIGURE 2. Simulated S-Parameters for the proposed 4G antennas, Ref1 (An1 w/o C_cap) and Ref2 (Ant1 w/o parasitic branch F_1G_1).

Ref2 antennas. The simulation results show that the reference antenna Ref1 generates six resonant modes at 0.59 GHz, 0.89 GHz, 1.50 GHz, 1.82 GHz, 2.40 GHz and 2.64 GHz, respectively. They are mode 1, mode 2, mode 3, mode 4 and mode 5, and mode 6. The circumference of the loop structure is approximately 243.5 mm. Because the resonance length of the fundamental mode of the slitted loop structure (with a breakpoint D_1 in the loop structure) is 0.5λ, and considering the influence of the FR4 substrate, the reference antenna Ref1 will produce a resonance mode at approximately 0.59 GHz, that is, mode 1. Mode 3, mode 4 and mode 5 are the higher order modes of the loop structure, which are a 1λ mode, 1.5λ mode and 2λ mode, respectively. Due to the existence of breakpoint D_1 in the loop structure, the monopole mode, namely mode 2, is generated by the branch strip formed by $A_1B_1C_1D_1$ at the frequency of 0.89 GHz. By introducing the lumped capacitance C_cap based on reference antenna Ref1, it can be seen that the resonant frequencies of mode 1 and mode 2 of Ant1 can be tuned to the desired frequency band, and the matching characteristics of mode 1 and mode 2 are greatly improved. The antenna matching characteristics of mode 4, which is the high order mode of mode 1, have also been significantly improved. In addition, from the comparison of reference antenna Ref2 and antenna Ant1, it can be seen that the resonant mode 6 comes from the dipole mode formed by the parasitic branch strip $B_1A_1F_1G_1$.

To better understand the working mechanism of the 4G antenna, Figs. 3(a) - (f) show the current distribution of antenna Ant1 in six resonant modes of frequency 0.86 GHz, 0.92 GHz, 1.56 GHz, 1.96 GHz, 2.38 GHz and 2.64 GHz. As shown in Fig. 3 (a), the current has a zero near the breakpoint D_1 of the loop structure, indicating that mode 1 is the 0.5λ loop mode [15]. Fig. 3 (b) shows that the current of mode 2 is mainly distributed on the branch strip formed by $A_1B_1C_1D_1$, corresponding to the monopole mode of 0.25λ. Similar to the analysis in Fig. 3 (a), Fig. 3 (c), Fig. 3 (d) and Fig. 3 (e) correspond to the higher order modes of the loop structure, i.e., the loop modes of 1λ, 1.5λ and 2λ [15], [16]. Fig. 3 (f) shows that the current of 2.64 GHz is mainly concentrated on the parasitic branch strip $B_1A_1F_1G_1$, corresponding to the dipole mode of 0.5 λ.

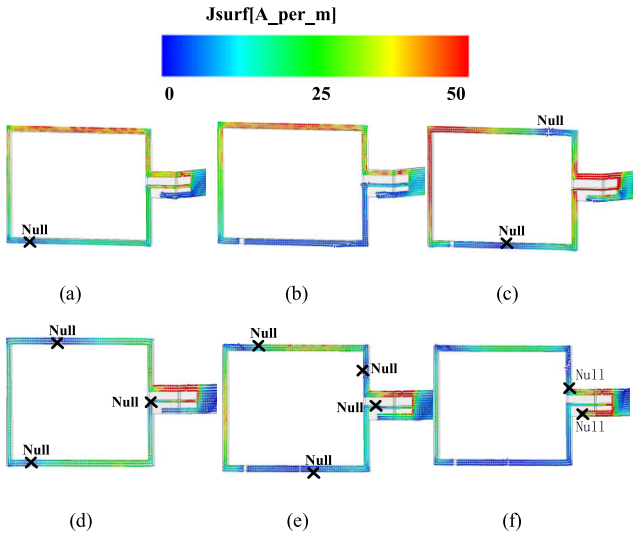

FIGURE 3. Current distribution paths of Ant1. (a) mode 1 at 0.86 GHz. (b) mode 2 at 0.92 GHz. (c) mode 3 at 1.56 GHz. (d) mode 4 at 1.96 GHz. (e) mode 5 at 2.38 GHz. (f) mode 6 at 2.64 GHz.

From the above description of a single 4G antenna, it can be seen that a single 4G antenna uses only one frame of the glasses in the design of the antenna structure, which just reserves the other frame of the glasses for the design of the other 4G antenna. Because of the symmetry of the two frames of the glasses, the symmetry of the two 4G antennas (Ant1, Ant2) is also guaranteed. There is an FR4 substrate with a distance of 20 mm between the two 4G antennas, which ensures sufficient isolation between the two 4G antennas. As seen from the results in Fig. 2, the isolation between two 4G antennas is better than 9.5 dB in the low frequency band and 20 dB in the high frequency band, which is enough for mobile terminal antennas.

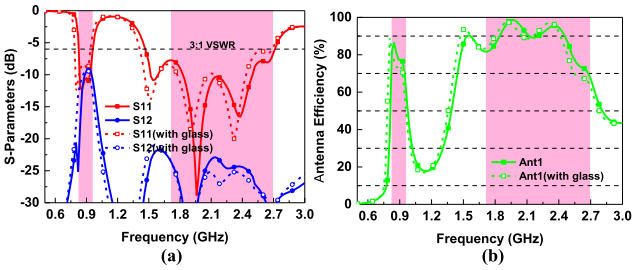

FIGURE 4. Simulated antenna parameters for 4G antennas with glasses. (a) S-Parameters, (b) antenna efficiency (including mismatching loss).

Considering the poor processing of glasses lenses, there are no glasses lenses in the antenna structure designed in this paper. For the influence of glasses lenses on antenna performance, the corresponding results are given by HFSS simulation software. In the simulation model, the size of the lens is 58 mm × 40 mm × 0.6 mm, and the relative dielectric constant is 5.5. The simulation results of Fig. 4 show that the effect of glasses lenses on the 4G antenna is very small. This conclusion is also applicable to 5G antenna, and the corresponding results are not given in this paper.

B. 5G GLASSES ANTENNAS

Four 5G slot antennas are printed on the two glasses legs modeled as FR4 substrates. The specific structure and size are shown in Fig. 5 (a). Because Ant3 is the same as Ant4 and Ant5 is the same as Ant6, only a part of the symmetric structure is given here. Both Ant3 and Ant5 are open-ended slots with sizes of 1.5 mm × 9.2 mm and 2 mm × 9.5 mm, respectively. The distance between Ant3 and Ant1 is 14 mm and the distance between Ant3 and Ant5 is 28.5 mm. Although the two antennas work in the same frequency band, their sizes are different. The reason is that the positions of antennas Ant3 and Ant5 in the whole glasses leg structure are different and asymmetric [17]. In addition, the same matching circuits are added in Ant3 and Ant5. The matching circuits are first connected with a 2.5-nH inductor L1 in parallel and then with a 1.0-nH inductor L2 in series.

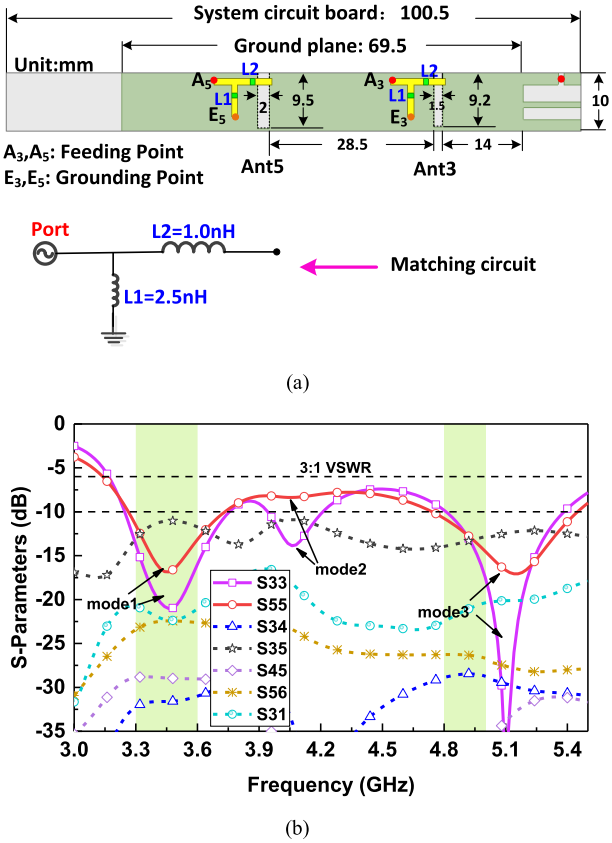

FIGURE 5. (a) Detailed dimensions and matching equivalent circuit of 5G antennas. (b) Simulated S-Parameters for 5G antennas.

Next, HFSS V15 is also used to analyze the resonant modes of the proposed 5G antennas. Fig. 5 (b) shows the simulation results of S-parameters of Ant3 and Ant5. From the simulation results, it can be seen that both Ant3 and Ant5 generate three modes – mode 1, mode 2 and mode 3, respectively, at 3.48 GHz, 4.0 GHz and 5.2 GHz. All three resonant modes are mainly attributed to the contribution of the open slot. In the excitation of mode 1, the coupling current on the ground plane near the microstrip feeding also plays a certain role. The excitation of mode 2 and mode 3 mainly comes from the fundamental mode of the open slot, but the excitation of the open slot for mode 2 and mode 3 is slightly different. In addition, only Ant3 and Ant5 in 5G antennas are close to each other, and the isolation between them is approximately 11 dB. The isolation between the other antennas is better than 20 dB.

The working mechanism of the resonant modes of the above 5G antennas is further verified by the corresponding current distribution and electric field distribution, as shown in Fig. 6. As seen from Fig. 6, the electric field distribution of the three modes of mode 1, mode 2 and mode 3 in the open slot is relatively concentrated, indicating that the open slot plays a major role in all three modes. Slightly different, in the excitation of mode 1, the current on the ground plane near the microstrip feeding is also obvious. Although the electric field distribution of mode 2 and mode 3 on the open slot presents the field distribution pattern of the fundamental mode, the specific field distribution is slightly different.

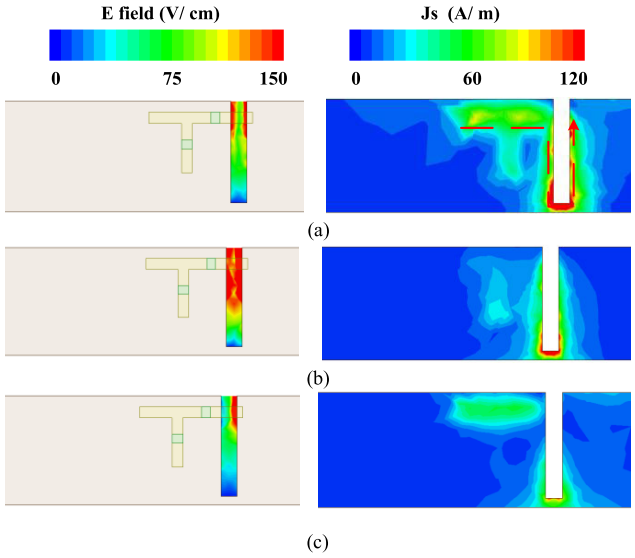

FIGURE 6. Simulated electric field distributions in the open slot, and surface current distributions on the ground plane of Ant3 at different resonant frequencies. (a) 3.48GHz. (b) 4.0GHz. (c) 5.2GHz.

For the matching circuits used in 5G antennas, their main functions are to improve the matching of 5G antennas, which can be proved by a set of curves in Fig. 7. The simulated results in Fig. 7 show that besides improving the antenna matching, the matching circuits can also tune the resonant frequencies of the resonant mode, especially mode 3.

Fig. 8 shows the S-parameter of Ant3 as a function of slot length. It can be seen from fig. 8 (a) that the slot length is also an important factor affecting its resonant frequencies and bandwidth. The longer the slot length is, the more the resonance frequencies of the antenna shifts to the low frequencies, and the wider the bandwidth of the antenna is. At the same time, the length fluctuation of Ant3 will also affect the isolation of Ant3 and Ant 5. Fig. 8 (b) shows that the

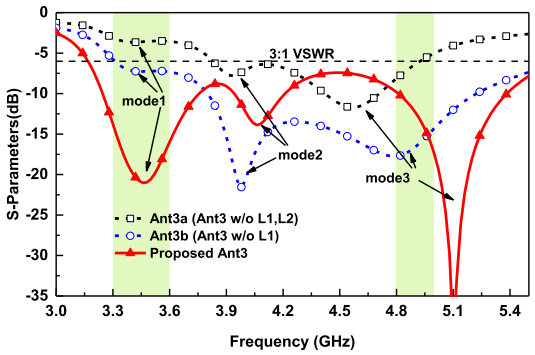

FIGURE 7. Simulated S-Parameters for the proposed 5G antenna Ant3, Ant3a (An3 w/o L1, L2) and Ant3b (Ant3 w/o L1).

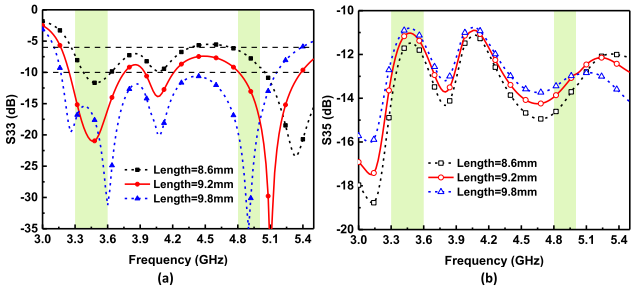

FIGURE 8. Simulated S-Parameters as a function of the length slot for the proposed 5G antenna Ant3, (a) S33, (b) S35.

longer the slot length is, the larger the value of S-parameter S35 is, that is, the smaller the isolation of the two antennas is. Combined with the above two factors, the slot length of Ant 3 is 9.2mm, its bandwidth can cover 3.3-3.6GHz and 4.8-5GHz, and the isolation between Ant3 and Ant 5 is also higher than 11dB.

Similar to the design of two 4G antennas, the design of four 5G antennas also takes full advantage of the symmetry of the glasses structure. That is, two 5G antennas, Ant3 and Ant5, are arranged on one glasses leg, and the other two 5G antennas, Ant4 and Ant6, are arranged on the other glasses leg. The distance between the two legs of the glasses is 166 mm, which ensures a high enough isolation between the 5G antennas Ant3 and Ant5 and the other two 5G antennas Ant4 and Ant6, which is higher than 20 dB. Although the distance between the two 5G antennas Ant3 and Ant5 is 28.5 mm, the isolation between them is still 11 dB.

III. USER'S HEAD EFFECTS

When the 4G/5G antennas applied to the glasses are actually working, they always face the situation that a human head is loaded around them. As a dielectric with high loss, the human body will have a great influence on the performance of the antenna [18], [19]. Therefore, the antenna performance under the loading state of the head model must also be carefully investigated to verify whether the proposed 4G/5G antenna is ultimately useful.

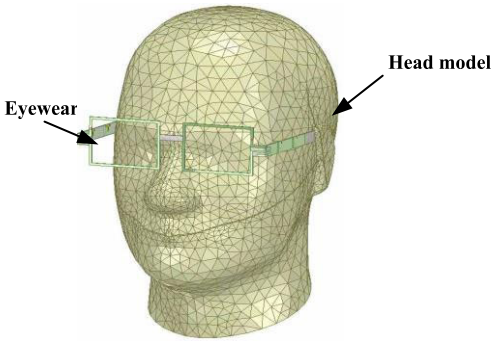

FIGURE 9. 4G/5G eyewear antennas on a head model.

Next, by means of simulation, the effects of a human head (SAM phantom [20] in Fig. 9) on 4G/5G antenna performance are studied, including S-parameters, antenna efficiency, envelope correlation coefficient (ECC), multiplexing Efficiency (ME).

A. S-PARAMETERS AND ANTENNA EFFICIENCY

First, the influence of the human head on the performance of 4G antennas is investigated. Fig. 10 shows the S-parameters and efficiency of the 4G antenna in free space and human head loading. As seen from Fig. 10 (a), compared with the antenna in free space, the resonance modes of the 4G antenna in the head-loaded state are the same, but the matching at some frequencies deteriorates slightly. From Fig. 10 (b), it can be seen that the efficiency of the 4G antenna in the head state deteriorates seriously, especially in the low frequency band 0.824-0.960 GHz. This is similar to what happened with mobile phone antennas [21]. Because the wavelengths of low frequency electromagnetic waves are longer, the head is more in the near field of the antenna, which naturally has a greater impact on the efficiency of the antenna.

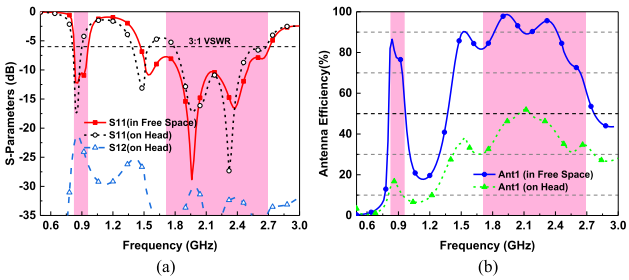

FIGURE 10. Simulated results of Ant1 in free space and on head. (a) S-Parameters, (b) antenna efficiency (including mismatching loss).

Fig. 11 shows the S-parameters and efficiency of 5G antennas in free space and human head loading. The effect of the human head on the 5G antenna is similar to that on the 4G antenna. In addition, the human head shown in Fig. 11 has a greater impact on Ant5 in the 5G antenna than

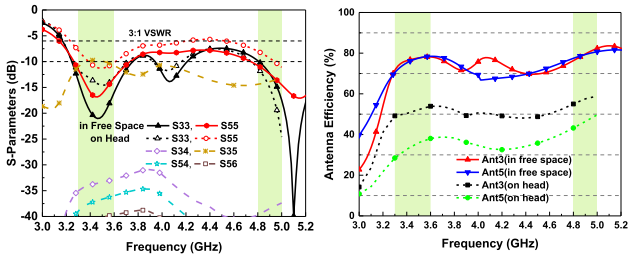

FIGURE 11. Simulated results of Ant3 and Ant5 in free space and on head. (a) S-Parameters, (b) antenna efficiency (including mismatching loss).

on Ant3 because the position of Ant5 in the glasses is closer to the human head.

B. CALCULATED ECC AND ME

For MIMO applications, the envelope correlation coefficient (ECC) [22], [23] between multiple antennas and the multiplexing efficiency (ME) [24] of multiple antennas are two important indicators to measure the performance of MIMO systems. Fig. 12 (a) and (b) show the simulation results of ECC and ME of the 4G/5G glasses antennas in both free space and human head model environments.

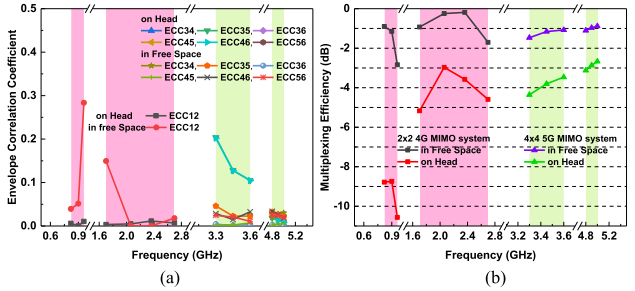

FIGURE 12. (a) Calculated ECCs of proposed 4G/5G eyewear antennas on head model and in free space. (b) compared the multiplexing efficiency performance of the proposed antenna array under two case.

As can be seen from Fig. 12 (a), in free space and human head model, the ECC between two 4G antennas is lower than 0.28 and 0.16 in low and high frequency bands respectively, and the ECC between any two 5G antennas is lower than 0.21 and 0.03 in low and high frequency bands, respectively, which are less than 0.5 and meet the standard requirements of MIMO applications.

It can be seen from Fig. 12 (b), the multiplexing efficiency of the proposed 2 × 2 4G MIMO system in the free space environment is about −2dB in the low frequency band and −1dB in the high frequency band, respectively; the multiplexing efficiency of the proposed 4 × 4 5G MIMO system in the low frequency band and the high frequency band are about −1dB. Compared with free space, the multiplexing efficiency of 4G antennas loaded with head mode decreases by 8 dB and 3 dB in low frequency and high frequency bands, respectively. Compared with free space, the multiplexing efficiency of 5G antennas loaded with head mode decreases by 3 dB and 2 dB in low frequency band and high frequency band, respectively. Compared with the 4G antennas in free space, the multiplexing efficiency of the 4G antennas loaded with head mode decreases more. The main reason is that the head mode has a greater impact on the 4G antennas in low frequency band.

C. SAR SIMULATIONS AND ANALYSIS

Considering that smart glasses are worn on the head in practical use, the electromagnetic radiation parameters SAR of antenna-to-head must be evaluated. Four representative simulated 1g SAR patterns are located at the top of Table 1. Considering the symmetry of the 4G antennas and 5G antennas, Table 1 provides the two standard SAR limit (1g SAR [25] and 10g SAR [26]) of Ant1, Ant3 and Ant5 simulated by HFSS software. Two cases of SAR are considered. One is the normal wearing of glasses, namely, the feeds of 4G antenna Ant1, 5G antenna Ant3 and 5G antenna Ant5, respectively, are about 30 mm, 17 mm and 10 mm away from the head mode. Secondly, the smart glasses are moved 10 mm in the opposite direction to the head mode, that is, the feeds of 4G antenna Ant1, 5G antenna Ant3 and 5G antenna Ant5 are about 38 mm, 30 mm and 15 mm away from the head mode respectively.

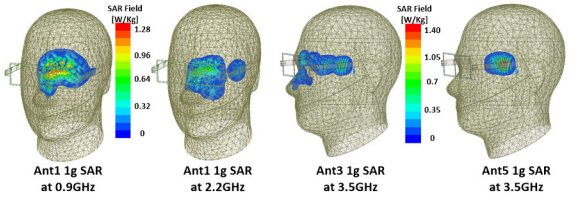

TABLE 1. Simulated result of SAR value.

-	Frequency	Input Power	1g SAR	10g SAR
-	(GHz)	(dBm)	(W/Kg)	(W/Kg)
Ant1	0.9	21	1.21#/0.93*	0.88#/0.64*
	2.2	21	0.93#/0.43*	0.67#/0.29*
Ant3	3.5	18	0.44#/0.16*	0.13#/0.07*
	4.9	18	0.88#/0.48*	0.32#/0.24*
Ant5	3.5	18	1.34#/0.79*	0.72#/0.46*
	4.9	18	1.56#/0.86*	0.84#/0.48*
Limit	-	-	**1.6**	**2**

Case1: 4G antenna source is 30 mm away from the head model, 5G antenna Ant3 is 17mm away from the head model, Ant5 is 10mm away from the head model; * Case2: 4G antenna source is 38 mm away from the head model; 5G antenna Ant3 is 30mm away from the head model, Ant5 is 15mm away from the head model.

From Table 1, it can be seen that the 1g SAR and 10g SAR values of the 4G antennas and 5G antennas at the selected frequency points are well below the limit in both cases. The SAR value of case 2 is slightly lower than that of case 1. For example, at 0.9 GHz, in case 2, 1g SAR and 10g SAR of 4G antenna Ant1 are 0.28W/kg and 0.24W/Kg lower than that of 4G antenna Ant1 in case 1, respectively.

At 3.5GHz, 1g SAR and 10g SAR of 5G antenna Ant3 in case 2 are 0.28W/kg and 0.06W/kg lower than 1g SAR and 10g SAR of 5G antenna Ant3 in case 1, respectively. 5G antenna Ant5 has similar phenomenon. This phenomenon shows that the SAR value is indeed related to the distance between the antenna and the head mode.

The head model is a large lossy medium, so the introduction of the head model will inevitably lead to a great loss of the radiation efficiency of the antenna. The absorption loss caused by the introduction of the head model can be expressed as the difference between the total efficiency of the antenna in free space and that of the loading head model. In addition, the mismatch loss of the antenna in the loading head model can be expressed as the difference between the total efficiency of the antenna and the radiation efficiency of the antenna. Table 2 shows the mismatch loss and absorption loss of 4G antenna Ant1 and 5G antenna Ant3 when loading head models respectively. From Table 2, it can be seen that the mismatch losses of 4G antenna and 5G antenna in loading head model are not large, generally less than 1dB, and only one case reach 1.4dB. However, the absorption losses caused by loading head model are quite large, some even as high as 7.6dB.

TABLE 2. Mismatch loss and absorption loss on head.

		Freq / Effi(dB) (GHz)	T-E*	T-E#	R-E#	M-L	A-L
4G	Low	*0.84*	-0.71	-7.93	-7.80	-0.13	7.22
		0.90	-1.12	-8.73	-7.33	-1.40	7.61
	High	*1.95*	-0.06	-3.32	-3.21	-0.11	3.26
		2.20	-0.43	-3.18	-2.82	-0.36	2.75
		2.45	-0.20	-4.30	-3.60	-0.70	4.10
5G	Low	*3.4*	-1.16	-2.98	-2.21	-0.77	1.82
		3.5	-1.09	-2.82	-2.23	-0.59	1.73
	High	*4.8*	-1.18	-2.60	-1.86	-0.74	1.42
		4.9	-0.86	-2.30	-2.04	-0.26	1.44

T-E=Total Efficiency,* in Free Space, # on Head;R-E=Radiation Efficiency, # on Head;M-L=Mismatch loss on Head; A-L=Absorption loss on Head.

IV. FABRICATING AND MEASUREMENT

The proposed 4G/5G glasses antennas have been fabricated, and the prototype is shown in Fig. 13. Fig. 14 gives the S-parameters of sim-ulation and measured of the 4G antennas and 5G antennas in free space, and their S-parameters on real human head are also shown in two figures. From Fig. 14 (a), it can be seen that the measured and simulated S-parameters of the 4G antennas are in good agreement, but some of the measured and simulated resonance frequencies are not in good agreement. From Fig. 14 (b), it can be seen that the S-parameters measured and simulated by Ant5 of the 5G antenna are in good agreement, but the S-parameters measured and simulated by Ant3 are quite different. The data errors of the above measurement and simulation may

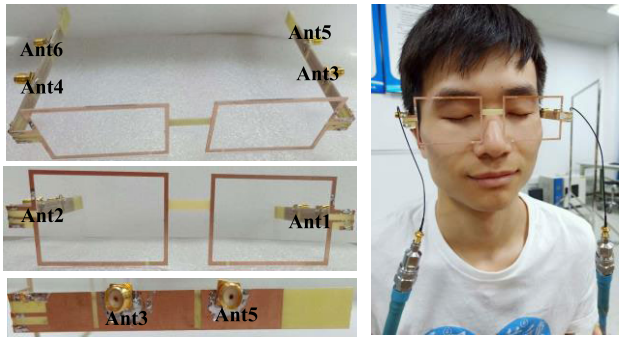

FIGURE 13. Photographs of the fabricated proposed 4G/5G eyewear antennas.

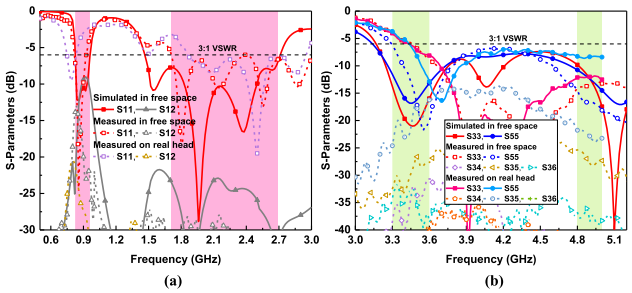

FIGURE 14. Measured and simulated S-Parameters of the proposed eyewear antennas. (a) 4G Ant1, (b) 5G Ant3 and Ant5.

come from the difference between the actual processing value and the simulation value of the dielectric constant of the FR4 substrate, the difference between the actual value and the simulation value of lumped inductance in the matching circuit, the difference between the actual processing size of antenna slot and the simulation value, and the introduction of a measure coaxial cable in the actual model for the need of measurement, etc.

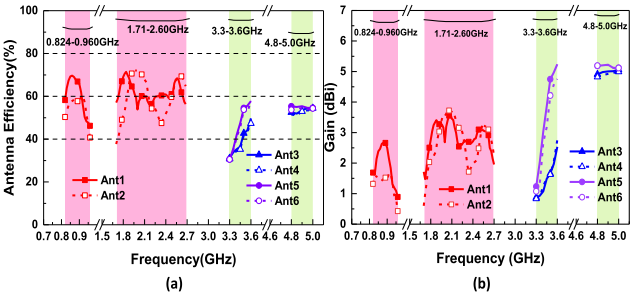

FIGURE 15. Measured result for the proposed eyewear antennas. (a) antennas efficiency, (b) antennas gain.

Fig. 15 shows the measured efficiency and gain of the 4G/5G glasses antennas. As shown in the fig. 15 (a), the low band efficiency of the 4G antenna is 40%-69%, and the high band efficiency is 53%-71%. The efficiency of the 5G antennas is 30%-57% in the 3.3-3.6 GHz band and 51%-54% in the 4.8-5.0 GHz band. As for the measured gain of the proposed antennas as shown in Fig. 15 (b), the measured gain

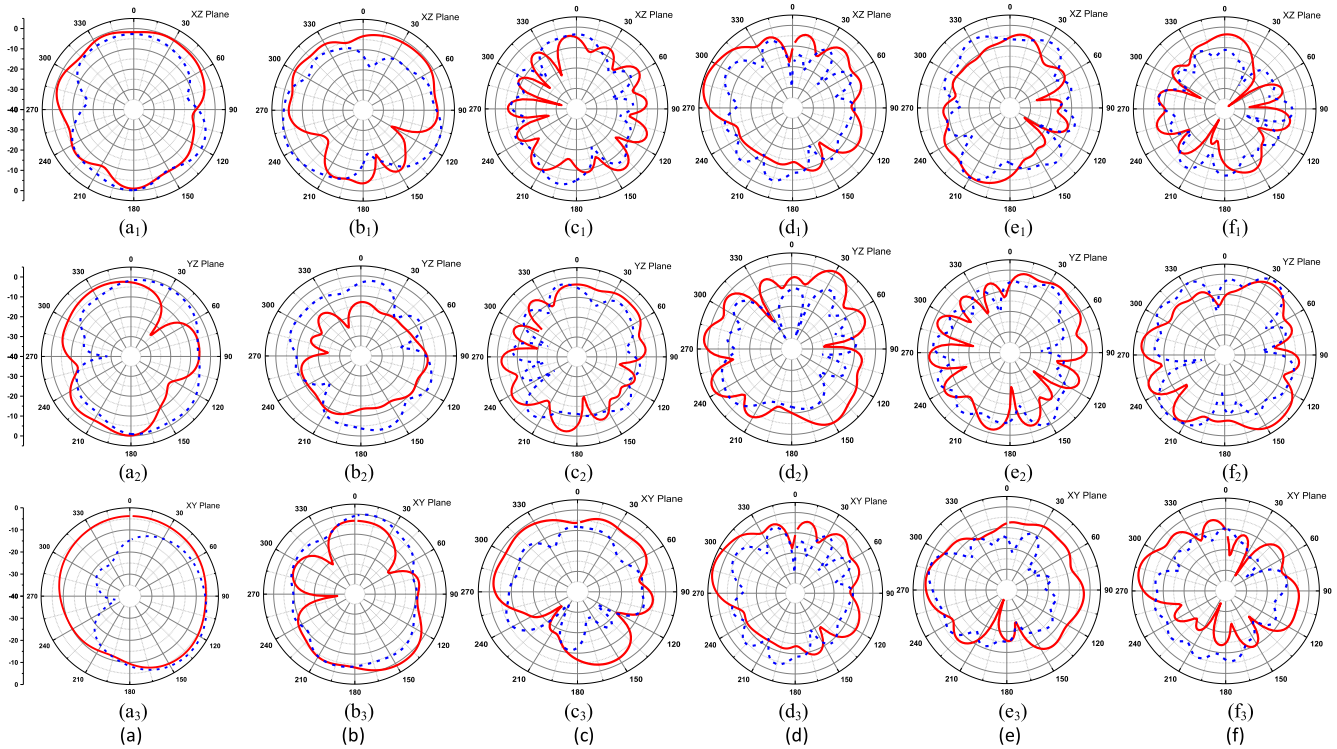

FIGURE 16. Measured 2-D radiation patterns of the proposed eyewear antenna (red line is Eφ, blue dash line is Eθ, unit: dB) at three principal planes. (a) Ant1 at 0.860GHz, (b) Ant1 at 2.380GHz, (c) Ant3 at 3.45GHz, (d) Ant3 at 5.2GHz, (e) Ant5 at 3.45GHz, (f) Ant5 at 5.2GHz.

of 4G antennas in low band and high band are 0.4-2.7 dBi and 0.6-3.7 dBi, respectively. And the measured gain of 5G antennas is 0.8-5.2 dBi in low band and 4.8-5.2 dBi in high band. These gain results agree well with theirs efficiency results shown in Fig. 15 (a). Compared with smartphones or other application devices [27], [28], such measurement results are acceptable for mobile wearable devices.

Fig. 16 shows the radiation patterns of 4G antenna Ant1 and 5G antennas Ant3, Ant5 in the xz plane, yz plane and xy plane, respectively. The radiation patterns of 4G antenna exhibited in xz plane, yz plane and xy plane are similar to [12]. The low-frequency at 0.860GHz has exhibited good near-omnidirectional pattern, and the defects (nulls) appear in the radiation patterns of high frequencies are similar to most reported LTE/WWAN antennas. Ant3 and Ant5 work at 5G bands, and the omnidirectional is not very good.

It should be noted in particular that, since there is no head model in our laboratory, it is not possible to measure the efficiency and MIMO performance of the antennas loading head model in the anechoic chamber.

Compared with the reference papers, the 4G loop antenna proposed in this paper is the only 2 × 2 MIMO antenna array formed by combining the structure of glass frame. However, most of the reference works [1], [3], [7], [9] – [11] integrate the antenna into the glasses leg area. The radiation elements of these works are very close to the human head, which is also the reason why the performance of the antenna loaded with head phantom is very undesirable. As shown in Table 3, the simulated antenna efficiency of reference [10] across LTE low band is very low, only 5% - 11%. In contrast, the simulated efficiency of the proposed antenna loaded with

TABLE 3. Comparison between proposed work and references.

Ant	Ant. type	Apply to	Operating band /BW (GHz)	Efficiency (%)	Gain (dBi)	MAI
[1]	Mono/ Loop	glasses	2.4 GHz WLAN/ Mono: 2.32-2.35$^{\#}$ loop: 2.35-2.5$^{\#}$	Mono: >10.7^ Loop: >33.9^	Mono:-11.6dBi Loop: -2.7dBi	Yes
[3]	IFA	glasses	2.4 GHz ISM/ 2.43-2.48*	23^	-1.08dBi	Yes
[7]	CE	glasses	LTE/ 0.7-0.96$^{\#}$, 1.7-2.7$^{\#}$	LB:10–12^, HB:20–35^		No
[9]	Dual-CE	glasses	LTE/ 0.7-0.96$^{\#}$, 1.7-2.7$^{\#}$	Ant1: LB:5–7^, HB:24–28^ Ant2: LB:9–21^, HB: 30–44^	Ant1: 5.78dBi Ant2: 4.35dBi	Yes
[10]	CE	glasses	LTE /0.72-0.96$^{\#}$, 1.32-2.4$^{\#}$	LB: 28–58$^{@}$, HB:42–65$^{@}$ LB: 5–9^, HB:18–31^	LB:-4.42dBi HB: 1.21dBi	No
[11]	CE	glasses	LTE/ 0.7-2.7$^{\#}$	LB: 55–60$^{@}$, HB: 45–58$^{@}$ LB: 7–9^, HB:9–23^	LB: -3.75dBi HB: 1.66dBi	No
This work	Loop/ Slot	glasses	LTE/ 0.82-0.96$^{\#}$, 1.48-2.70$^{\#}$	LB: 54.5–86.5$^{@}$, HB: 67–98.6$^{@}$ LB: 10–20^, HB: 30–52^	LB: 2.67dBi HB: 3.72dBi	Yes

Mono = Monopole; BW=Bandwidth; CE = Coupling Element; $^{\#}$ = -6 dB BW, * = -10 dB BW; $^{@}$in free space, ^on the head phantom (simulation); MAI = Multi-Antenna Implementation; IFA = Inverted-F Antennas.

head phantom is at least 18% across the low band. Finally, 5G antennas and the MIMO technology are the inevitable trend of future communication development, but reference antennas [7], [10] and [11] are not of the MIMO antenna types, and even though [9] investigated a dual- coupling element (CE) for a 4G eyewear antenna, the MIMO performance of [9] was not studied. At the same time, 5G antenna design is not included in these reference works. Therefore, our proposed work exhibits better performance (including MIMO performance) in the expected 4G and 5G frequency bands.

V. CONCLUSION

This paper provides a glasses MIMO antenna scheme for 4G/5G communication. The specific concept of this scheme is that two antennas for 4G communication are laid on two glasses frames and four antennas for 5G communication are laid on two glasses legs. The advantage of this arrangement is that it makes full use of the limited three-dimensional space structure provided by glasses and achieves the perfect combination of antenna and glasses in the physical structure. In this paper, the design idea and principle of 4G/5G antennas are discussed in detail. Samples were fabricated and measured. The measured results show that the proposed antennas perform well and have potential to be used in 4G/5G communications employing glasses.

REFERENCES

[1] A. Cihangir, F. Gianesello, and C. Luxey, "Dual-antenna concept with complementary radiation patterns for glasses applications," *IEEE Trans. Antennas Propag.*, vol. 66, no. 6, pp. 3056–3063, Jun. 2018.

[2] Y.-F. Zheng, G.-H. Sun, Q.-K. Huang, S.-W. Wong, and L.-S. Zheng, "Wearable PIFA antenna for smart glasses application," in *Proc. IEEE Int. Conf. Comput. Electromagn. (ICCEM)*, Guangzhou, China, Feb. 2016, pp. 370–372.

[3] S. Choi and J. Choi, "Miniaturized MIMO antenna with a high isolation for smart glasses," in *Proc. IEEE-APS Top. Conf. Antennas Propag. Wireless Commun. (APWC)*, Verona, Italy, Sep. 2017, pp. 61–63.

[4] S. Hong, S. H. Kang, Y. Kim, and C. W. Jung, "Transparent and flexible antenna for wearable glasses applications," *IEEE Trans. Antennas Propag.*, vol. 64, no. 7, pp. 2797–2804, Jul. 2016.

[5] H. Raad, C. White, H. Schmitzer, D. Tierney, A. Issac, and A. Hammoodi, "A 2.45 GHz transparent antenna for wearable smart glasses," in *Proc. Prog. Electromagn. Res. Symp.-Fall (PIERS-FALL)*, Singapore, Nov. 2017, pp. 99–102.

[6] S. Sayah and R. Sarkis, "Design and analysis of conformal antennas for smart watch," in *Proc. Prog. Electromagn. Res. Symp.-Fall (PIERS-FALL)*, Singapore, Nov. 2017, pp. 1889–1894.

[7] A. Cihangirl, W. G. Whittow, C. J. Panagamuwa, F. Ferrero, G. Jacquemod, F. Gianesello, and C. Luxey, "Feasibility study of 4G cellular antennas for eyewear communicating devices," *IEEE Antennas Wireless Propag. Lett.*, vol. 12, pp. 1704–1707, 2013.

[8] S. Wang, H. Arai, A. Cihangir, and C. Luxey, "Characteristic modes analysis of A 4G cellular antenna for eyewear wireless devices," in *Proc. IEEE Int. Workshop Electromagn. (iWEM)*, Sapporo, Japan, Aug. 2014, pp. 16–17.

[9] A. Cihangirl, C. Luxey, G. Jacquemod, R. Pilard, F. Gianesello, W. G. Whittow, and C. J. Panagamuwa, "Investigation of the effect of metallic frames on 4G eyewear antennas," in *Proc. Loughborough Antennas Propag. Conf. (LAPC)*, Loughborough, U.K., 2014, pp. 60–63.

[10] A. Cihangirl, C. J. Panagamuwa, W. G. Whittow, G. Jacquemod, F. Gianesello, R. Pilard, and C. Luxey, "Dual-band 4G eyewear antenna and SAR implications," *IEEE Trans. Antennas Propag.*, vol. 65, no. 4, pp. 2085–2089, Apr. 2017.

[11] A. Cihangir, C. J. Panagamuwa, W. G. Whittow, F. Gianesello, and C. Luxey, "Ultrabroadband antenna with robustness to body detuning for 4G eyewear devices," *IEEE Antennas Wireless Propag. Lett.*, vol. 16, pp. 1225–1228, 2017.

[12] K.-L. Wong and Y.-C. Chen, "Small-size hybrid loop/open-slot antenna for the LTE smartphone," *IEEE Trans. Antennas Propag.*, vol. 63, no. 12, pp. 5837–5841, Dec. 2015.

[13] I. R. R. Barani and K.-L. Wong, "Integrated inverted-F and open-slot antennas in the metal-framed smartphone for 2×2 LTE LB and 4×4 LTE M/HB MIMO operations," *IEEE Trans. Antennas Propag.*, vol. 66, no. 10, pp. 5004–5012, Oct. 2018.

[14] ANSYS. (2015). *ANSYSHFSS*. [Online]. Available: hppt://www.ansys.com/staticassets/ANSYS/staticassets/resourcelibrary/brochure/ansyshfss-brochure-16.0.pdf

[15] H. Xu, H. Wang, S. Gao, H. Zhou, Y. Huang, Q. Xu, and Y. Cheng, "A compact and low-profile loop antenna with six resonant modes for LTE smartphone," *IEEE Trans. Antennas Propag.*, vol. 64, no. 9, pp. 3743–3751, Sep. 2016.

[16] L.-W. Zhang, Y.-L. Ban, C.-Y.-D. Sim, J. Guo, and Z.-F. Yu, "Parallel dual-loop antenna for WWAN/LTE metal-rimmed smartphone," *IEEE Trans. Antennas Propag.*, vol. 66, no. 3, pp. 1217–1226, Mar. 2018.

[17] Y.-L. Ban, C. Li, C.-Y.-D. Sim, G. Wu, and K.-L. Wong, "4G/5G multiple antennas for future multi-mode smartphone applications," *IEEE Access*, vol. 4, pp. 2981–2988, 2016.

[18] A. Cihangir, F. Ferrero, G. Jacquemod, P. Brachat, and C. Luxey, "Neutralized coupling elements for MIMO operation in 4G mobile terminals," *IEEE Antennas Wireless Propag. Lett.*, vol. 13, pp. 141–144, 2014.

[19] M. Stanley, Y. Huang, H. Wang, H. Zhou, Z. Tian, and Q. Xu, "A novel reconfigurable metal rim integrated open slot antenna for octa-band smartphone applications," *IEEE Trans. Antennas Propag.*, vol. 65, no. 7, pp. 3352–3363, Jul. 2017.

[20] C. Gabriel, "Tissue equivalent material for hand phantoms," *Phys. Med. Biol.*, vol. 52, 14, pp. 4205–4210, Jun. 2017.

[21] C. I. Lin and K. L. Wong, "Printed monopole slot antenna for internal multiband mobile phone antenna," *IEEE Trans. Antennas Propag.*, vol. 55, no. 12, pp. 3690–3697, Dec. 2007.

[22] R. G. Vaughan and J. B. Andersen, "Antenna diversity in mobile communications," *IEEE Trans. Veh. Technol.*, vol. VT-36, no. 4, pp. 149–172, Nov. 1987.

[23] Y. Ding, Z. Du, K. Gong, and Z. Feng, "A novel dual-band printed diversity antenna for mobile terminals," *IEEE Trans. Antennas Propag.*, vol. 55, no. 7, pp. 2088–2096, Jul. 2007.

[24] R. Tian, B. K. Lau, and Z. Ying, "Multiplexing efficiency of MIMO antennas," *IEEE Antennas Wireless Propag. Lett.*, vol. 10, pp. 183–186, 2011.

[25] *Human Exposure to Radio Frequency Fields From Hand-Held and Body-Mounted Wireless Communication Devices—Human Models, Instrumentation, and Procedures—Procedure to Determine the Specific Absorption Rate (SAR) for Hand-Held Devices Used in Close Proximity to the Ear (Frequency Range of 300 MHz to 3 GHz)*, document IEC 62209-1:2005, 2005.

[26] *IEEE Recommended Practice for Determining the Peak Spatial-Average Specific Absorption Rate (SAR) in the Human Head From Wireless Communications Devices: Measurement Techniques*, IEEE Standard 1528-2003, Sep. 2013.

[27] Y. Li, C.-Y.-D. Sim, Y. Luo, and G. Yang, "12-port 5G massive MIMO antenna array in sub-6 GHz mobile handset for LTE bands 42/43/46 applications," *IEEE Access*, vol. 6, pp. 344–354, Oct. 2017.

[28] R. K. Saraswat and M. Kumar, "A metamaterial hepta-band antenna for wireless applications with specific absorption rate reduction," *Int. J. RF Microw. Comput. Aided Eng.*, vol. 29, no. 10, p. e21824, 2019, doi: 10.1002/mmce.21824.

YAN-YAN WANG was born in Henan, China, in September 1992. She received the B.S. degree in communication engineering from the North China University of Water Resources and Electric Power, Zhengzhou, China, in 2017. She is currently pursuing the M.S. degree with the University of Electronic Science and Technology of China (UESTC), Chengdu, China. Her current research interest includes multiband smart wearable antennas for wireless communications, especially 4G/5G antenna designs for smart glasses.

YONG-LING BAN was born in Henan, China. He received the B.S. degree in mathematics from Shandong University, the M.S. degree in electromagnetics from Peking University, and the Ph.D. degree in microwave engineering from the University of Electronic Science and Technology of China (UESTC), in 2000, 2003, and 2006, respectively. In July 2006, he joined the Xi'an Mechanical and Electric Information Institute as a Microwave Engineer. Then, he joined Huawei Technologies Co., Ltd., Shenzhen, China. At Huawei, he designed and implemented various terminal antennas for 15 data card and mobile phone products customized from leading telecommunication industries like Vodafone. From September 2010 to July 2016, he was an Associate Professor with UESTC, where he is currently a Professor. From May 2014 to April 2015, he visited the Queen Mary University of London as a Scholar Visitor. His research interests include wideband small antennas for 4G/5G handset devices, MIMO antenna, and millimeter wave antenna array. He has authored more than 110 refereed journal and conference papers on these topics. He holds 20 granted and pending Chinese and overseas patents.

YANHUI LIU (M'15–SM'19) received the B.S. and Ph.D. degrees in electrical engineering from the University of Electronic Science and Technology of China (UESTC), Chengdu, China, in 2004 and 2009, respectively. From 2007 to 2009, he was a Visiting Scholar with the Department of Electrical Engineering, Duke University, Durham, NC, USA. In 2011, he joined the Department of Electronic Science, Xiamen University, Xiamen, China, where he is currently a Full Professor. In 2017, he was a Visiting Professor with the State Key Laboratory of Millimeter Waves, City University of Hong Kong, Hong Kong. Since 2017, he has been as a Visiting Professor/Research Principal with the Global Big Data Technologies Centre, University of Technology Sydney (UTS), Ultimo, NSW, Australia. He has authored and coauthored more than 130 peer-reviewed journals and conference papers. He holds several granted Chinese invention patents. His current research interests include antenna array design, reconfigurable antennas, and electromagnetic signal processing.

Dr. Liu has served as a TPC Member or Reviewer (many times) for the IEEE APS, PIERS, APCAP, and NCANT. He was a recipient of the UESTC Outstanding Graduate Award, in 2004, and the Excellent Doctoral Dissertation Award of Sichuan Province of China, in 2011. He served as a Session Chair for NCANT2015, PIERS2016, ACES2017-China, NCANT2017, APCAP2017, and ICCEM2018/2019. Since 2018, he has been serving as an Associate Editor for IEEE Access. He is serving as a Reviewer for a dozen of SCI-indexed journals.